

A Journal of the Gesellschaft Deutscher Chemiker

# Angewandte Chemie

GDCh

International Edition

www.angewandte.org

## Accepted Article

**Title:** Craig-Hückel Hybrid Aromatic Metalla-dehydro[11]annulenes Constructed by a Formal [10+1] Cycloaddition Reaction

**Authors:** Kaidong Ruan, Zhengyu Lu, Ren Rao, Jiao-Jiao Liu, Dafa Chen, and Haiping Xia

This manuscript has been accepted after peer review and appears as an Accepted Article online prior to editing, proofing, and formal publication of the final Version of Record (VoR). The VoR will be published online in Early View as soon as possible and may be different to this Accepted Article as a result of editing. Readers should obtain the VoR from the journal website shown below when it is published to ensure accuracy of information. The authors are responsible for the content of this Accepted Article.

**To be cited as:** *Angew. Chem. Int. Ed.* **2023**, e202316885

**Link to VoR:** <https://doi.org/10.1002/anie.202316885>

## RESEARCH ARTICLE

# Craig-Hückel Hybrid Aromatic Metalla-dehydro[11]annulenes Constructed by a Formal [10+1] Cycloaddition Reaction

Kaidong Ruan,<sup>[a,b]</sup> Zhengyu Lu,<sup>[b]</sup> Ren Rao,<sup>[a,b]</sup> Jiao-Jiao Liu,<sup>[b]</sup> Dafa Chen,<sup>\*,[b]</sup> and Haiping Xia<sup>\*,[a,b]</sup>

[a] K. Ruan, R. Rao, Prof. H. Xia

State Key Laboratory of Physical Chemistry of Solid Surfaces, College of Chemistry and Chemical Engineering

Xiamen University

Xiamen 361005, China

E-mail: xiahp@sustech.edu.cn

[b] K. Ruan, Dr. Z. Lu, R. Rao, J.-J. Liu, Prof. D. Chen, Prof. H. Xia

Shenzhen Grubbs Institute, Department of Chemistry

Southern University of Science and Technology

Shenzhen 518055, China

E-mail: chendf@sustech.edu.cn

Supporting information for this article is given via a link at the end of the document.

**Abstract:** Aromatic metalla-annulenes are important aromatic compounds, research into which has been mainly concentrated on metal-benzenes and their lower homologues. Reports on their superior homologs are rare, and this has greatly limited the systematic study of their properties. In this work, a series of osma-dehydro[11]annulenes with good air and thermal stability were prepared in high yields through a simple [10+1] strategy, by incorporating a metal fragment into conjugated ten-carbon chains in a one-pot reaction. They are the first monometallic aromatic metalla-[*n*]annulenes with the ring size larger than 6, and their Craig-Hückel hybrid aromaticity is supported by various physical and computational parameters. Besides, these complexes show versatile reactivities, not only giving further evidence for their aromaticity, but also demonstrating their physical and chemical properties can easily be regulated. This work enriches the metalla-aromatic chemistry, and provides a new avenue for the synthesis of large metalla-annulenes with different ring sizes.

## Introduction

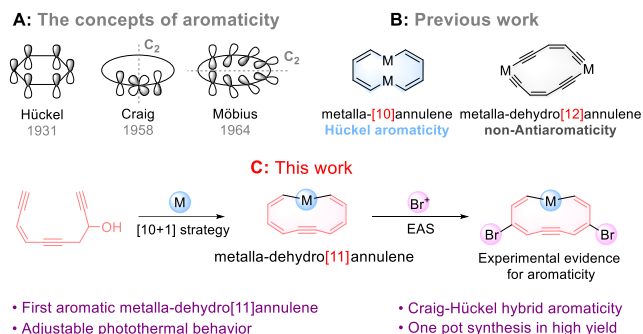
[*n*]Annulenes are interesting fully conjugated cyclic hydrocarbons with a general formula of C<sub>*n*</sub>H<sub>*n*</sub>, in which *n* represents the number of carbon atoms in the ring. Dehydro-annulenes are annulene derivatives from which at least two hydrogen atoms have been removed, and they are generally less stable than their parent annulenes.<sup>[1]</sup> As *n* increases, the out-of-plane distortion increases, leading to the decrease of the overlap between *p*-orbitals.<sup>[2]</sup> As a result, their 4*N*+2 Hückel aromaticity gradually weakens, but on the other hand, it may result in C<sub>2</sub>-symmetric 4*N* Möbius aromaticity with the property of orbital phase inversion.<sup>[3-5]</sup> For

example, in 2003, the Herges' group successfully synthesized a Möbius aromatic [16]annulene with a twisted molecular skeleton.<sup>[6]</sup> In addition to the above two types of aromaticity, Craig and his co-workers theoretically predicted another aromaticity in 1958.<sup>[7]</sup> Considering that orbital phase inversion might also be caused by *d*-orbitals, Craig *et al.* assumed if *d*-orbitals participated in conjugation, 4*N* Craig aromaticity with a planar molecular skeleton and C<sub>2</sub>-symmetry might be obtained (Scheme 1A). However, Craig aromaticity cannot be realized in [*n*]annulenes due to the lack of *d*-orbitals that can participate in bonding. On the other hand, when transition metals are embedded in [*n*]annulenes, the achieved metalla-[*n*]annulenes might have Craig characteristics due to their *d*-orbitals.<sup>[8]</sup>

Since Thorn and Hoffman predicted the aromaticity of metalla-benzenes (i.e. metalla-[6]annulenes),<sup>[9]</sup> many of these substances and their lower homologues have been reported.<sup>[10]</sup> In contrast, their superior homologues are very rare. To our knowledge, such complexes with aromaticity discussed have only two types, dicupra-[10]annulenes<sup>[11]</sup> constructed by a [4+1+1+4] method reported by Xi *et al* and dirhena-dehydro[12]annulenes<sup>[12]</sup> synthesized through a [6+6] method by Jia *et al.* (Scheme 1B). Of these, the former were regarded to be Hückel aromatic by the authors, while the latter were considered to be non-antiaromatic, and both are dimetallic complexes. In order to expand the framework of metalla-[*n*]annulenes, herein, we prepared a series of metalla-dehydro[11]annulenes by adopting a simple [10+1] strategy, and systematically studied their interesting aromaticity from both experimental and theoretical aspects: they are Craig-Hückel hybrid aromatic complexes but dominated by Craig aromaticity (Scheme 1C). It is worth mentioning that they represent the first aromatic metalla-[*n*]annulene derivatives in

## RESEARCH ARTICLE

which  $n$  is an odd number  $> 6$ , and meanwhile, they are also the first monometallic aromatic metalla- $[n]$ annulenes with the ring size larger than 6. Notably, they have good thermal stability in air and exhibit good near-infrared photothermal properties.



**Scheme 1.** (A) The proposed concepts of aromaticity. (B) Reported metalla-[10]annulenes and metalla-dehydro[12]annulenes. (C) Our design to synthesize the aromatic metalla-dehydro[11]annulene.

## Results and Discussion

To construct the target metalla-dehydro[11]annulene, we planned to incorporate a metal fragment into a conjugated ten-carbon chain. Nevertheless, for an eleven-membered conjugated ring, its flexible conformation would make it difficult to be identified.<sup>[13]</sup> To solve this problem, we thought the introduction of a  $C\equiv C$  unit in the middle of the carbon chain, which can coordinate with the metal center and lock the entire conjugated macrocycle, could be very helpful. Consequently, the precursor **L1** with ten carbon atoms was designed. When **L1** was treated with  $OsCl_2(PPh_3)_3$  in the presence of  $CH_3COOH$  and  $PPh_3$  in  $CH_2Cl_2$  at room temperature (rt) for 10 min, a red solution was obtained. Attempts to purify this red product were unsuccessful due to its instability but further addition of  $P(OMe)_3$ , 2-isocyanonaphthalene, or 2,2'-bipyridine/ $AgBF_4$  led to isolable complexes (**1a**, **1b** and **1c**) in the yields of 91%, 93% and 86%, respectively (Figure 1A).

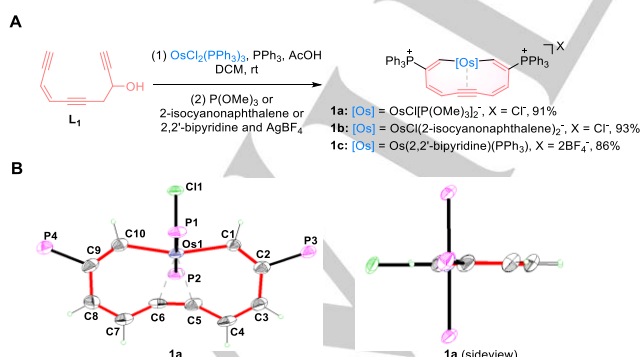


**Figure 1.** (A) Synthesis of osma-dehydro[11]annulenes **1a**, **1b** and **1c**. (B) Single-crystal X-ray structure for the cation of complex **1a** with thermal ellipsoids drawn at the 50% probability level. Phenyl groups in  $PPh_3$  and methoxy groups in  $P(OMe)_3$  have been omitted for clarity.

Complexes **1a**, **1b** and **1c** have the same basic skeleton, and here only complex **1a** is discussed. The X-ray crystal structure of **1a** shows that it has a  $C_{2v}$  symmetrical cation (Figure 1B). Moreover, it is a planar 11-membered metalla-cycle, in which the alkynyl group and the osmium metal interact. The 11-membered ring (11MR) has a beautiful goggles-like structure, and a sum of the internal bond angles of  $1620.0^\circ$ , identical to that of a planar hendecagon, and the mean deviation from the least-squares plane is  $0.023 \text{ \AA}$ . In addition to the alkynyl group, there are two *trans*  $P(OMe)_3$  groups, one Cl atom and two carbon atoms (C1 and C10) connected to the osmium center, forming an octahedral structure. To investigate the nature of interactions between the triple bond and the osmium atom, the known complex **I**<sup>[14]</sup> reported by Esteruelas *et al.* (Figure 2), in which the alkyne and the osmium center form an osma-cyclopropene, was used for comparison. In the  $^{13}C\{^1H\}$  NMR spectrum of **I**, both alkynyl carbons are coordinated with osmium providing a signal at 168.7 ppm. In comparison, the chemical shift of the corresponding carbon atoms (C5 and C6) of **1a** appears further upfield at 96.33 ppm, ruling out the possibility of three-membered ring  $Os1-C5-C6$  or an osma-cyclopropene in complex **1a**. In fact, the peak at 96.33 ppm is quite close to those of alkynyl carbons in cyclooctynes which are at 91-100 ppm.<sup>[15]</sup> In addition, the IR spectrum of **1a** shows a  $C5\equiv C6$  stretching absorption peak at  $1936 \text{ cm}^{-1}$ . Although this frequency is lower than that in known cyclic alkynes ( $2100$  to  $2200 \text{ cm}^{-1}$ ),<sup>[15]</sup> it is close to the  $C\equiv C$  absorption of a 1-zircona-2,5-disilacyclopent-3-yne ( $1899 \text{ cm}^{-1}$ )<sup>[16]</sup> which has a weakened bond between alkyne and metal, but is far from the  $1611 \text{ cm}^{-1}$  observed in a metalla-cyclopropene.<sup>[17]</sup> As a result, complex **1a** can be regarded simply as an osma-dehydro[11]annulene with weak interactions between its  $C\equiv C$  bond and osmium center.

In the  $^1H$  NMR spectrum of **1a**, the protons on the metal-bonded carbons (C1H and C10H) have a signal at 13.05 ppm, close to those of the protons *ortho* to the metal in the first metalla-benzene, osma-benzene (**II**) (13.95 ppm),<sup>[18]</sup> and another osma-benzene (**III**) (12.74 ppm),<sup>[19]</sup> but significantly downfield from that of the non-aromatic osma-cycle **IV** (7.08 ppm) (Figure 2).<sup>[20]</sup> In fact, the extremely downfield proton signals located in the region of 11-14 ppm are characteristic of metal *ortho*-protons in metalla-benzenes.<sup>[21]</sup> Furthermore, the chemical shifts of other four protons bonded to carbons in the 11MR are at 7.45 (C4H and C7H) and 7.23 (C3H and C8H) ppm, which are typical for aromatics rather than olefins. Therefore, the  $^1H$  NMR data support that **1a** is a metalla-aromatic complex.

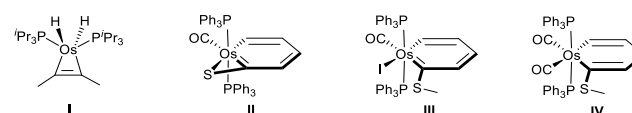


**Figure 2.** Molecular structures of **I-IV**.

To further confirm the aromaticity of **1a**, nucleus-independent chemical shift (NICS) calculations were performed on the model complex **1a'**, in which the  $P(OMe)_3$  ligands of **1a** are for the sake

## RESEARCH ARTICLE

of simplicity, regarded as  $\text{PH}_3$ , and the  $\text{PPh}_3^+$  substituents are omitted. Normally, aromatic complexes have negative NICS values, whereas antiaromatic complexes result in positive values. The NICS(1) $_{zz}$  index describing the  $zz$  component 1.0 Å above the ring center is adopted.<sup>[22]</sup> As shown in Figure 3A, The NICS(1) $_{zz}$  values of **1a'** at the ring center (point a) is -57.3 ppm, however, this significant negative value may not be credible because the distance between point a and osmium atom is less than the atomic radius of osmium atom, and this too close distance makes its NICS value not only affected by the shielding effect of clockwise ring current, but also by the shielding effect of osmium atom electrons, thus resulting in a more negative value.<sup>[23]</sup> Therefore, the point b, which represents the center of the six atoms on the left (one osmium and five carbon atoms in the 11MR) was further selected for the calculation. The NICS(1) $_{zz}$  value at point b is -23.9 ppm indicating obvious aromaticity.

The anisotropy of the induced current density (ACID) analysis, a widely used criterion of aromaticity, was further conducted (Figure 3B).<sup>[24]</sup> The diatropic ring current on the ACID isosurfaces in the  $\pi$  system of **1a'** is distinctly clockwise along the outer ring (a higher resolution figure is shown in Figure S14), revealing its  $\pi$  aromaticity. The  $zz$  component of the iso-chemical shielding surfaces (ICSS $_{zz}$ ) of **1a'** shows a shielding cone (green) in the ring and a deshielding loop (blue) out of the ring, which is consistent with the character of an aromatic complex (Figure 3C).<sup>[25]</sup>

The isomerization stabilization energy (ISE) method is another popular criterion for evaluation of aromaticity. An energy of -14.1 kcal·mol<sup>-1</sup> for **1a'** was provided using "methyl-methylene isomerization method",<sup>[26]</sup> and is also in agreement with its aromaticity (Figure 3D).

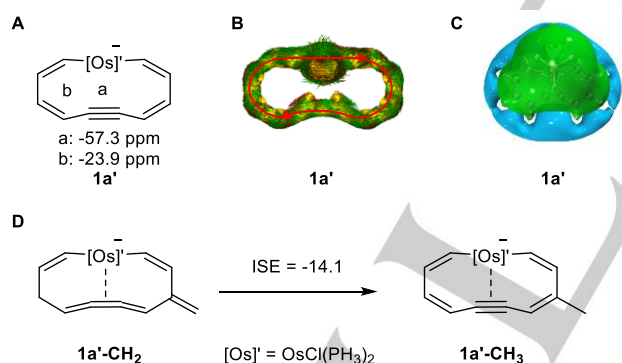


**Figure 3.** (A) The NICS(1) $_{zz}$  values (ppm) of the model compound **1a'**. (B) ACID isosurface of **1a'** from the  $\pi$  contribution. The ACID plots are visualized with an isosurface value of 0.04 a. u. The corresponding clockwise ring currents are displayed (red arrow). (C) The ICSS $_{zz}$  plots of **1a'** with an isosurface value of 5.0 ppm displaying shielding (green) and deshielding (blue) surfaces. (D) ISE evaluations of the aromaticity of **1a'** by methyl-methylene isomerization method (kcal/mol).

In order to gain more information on the origin of the aromaticity, the canonical molecular orbital (CMO) NICS calculations were carried out.<sup>[27]</sup> As shown in Figure 4A, the six  $\pi$

molecular orbitals ( $\pi$ -MOs) of **1a'**, three of which are  $C_2$  symmetric Craig-type (with  $d_{xz}$  involved) and three are plane symmetric Hückel-type (with  $d_{yz}$  involved), introduce an eleven-center aromatic system. Meanwhile, the NICS(1) $_{\pi,zz}$  value of the sum of Craig-type  $\pi$ -MOs at point b, -16.56 ppm, is nearly double that of Hückel-type  $\pi$ -MOs (-8.63 ppm), indicating it is a Craig-Hückel hybrid aromatic system, but is dominated by Craig aromaticity. Notably, the HOMO-7 is consistent with the Craig aromaticity model shown in the middle of Scheme 1A, revealing the  $d_{\pi}$ - $p_{\pi}$  conjugation for the bonding interaction of  $d_{xz}$  with  $p_z$ .

Moreover, electron density of delocalized bonds (EDDB) analysis was conducted to provide a more direct and comprehensive understanding of the delocalization of  $\pi$ -electrons in the molecular fragment.<sup>[28]</sup> This analysis also allows for determining the contribution of atom orbitals to the delocalized electrons. Specifically, we focused on calculating the number of delocalized  $\pi$ -electrons ( $\pi$ -EDDB( $r$ )) solely within the 11MR on **1a'**. To achieve this, we selected total natural orbitals for bond delocalization (NOBOs) with  $\pi$  symmetry (Figure S15). As depicted in Figure 4B, the total contribution of delocalized electrons within the 11MR amounts to 5.15 |e|, with the ten carbon atoms'  $2p_z$  orbitals accounting for 85% (4.36 |e|) (the average contribution per carbon atom is about 0.44 |e|). The remaining 15% (0.79 |e|) originates from the 5d orbitals of osmium, with contributions from both its  $5d_{xz}$  and  $5d_{yz}$  components amounting to approximately 12% (0.64 |e|) and 3% (0.15 |e|), respectively. The contribution of the osmium's 5d orbitals is greater than that of the  $2p_z$  orbital of a single carbon atom, suggesting that osmium plays a crucial role in electron delocalization within this system. Additionally, the dominance of Craig aromaticity has been further demonstrated, as evidenced by the contribution of  $5d_{xz}$  orbital being approximately four times greater than that of  $5d_{yz}$  orbital.

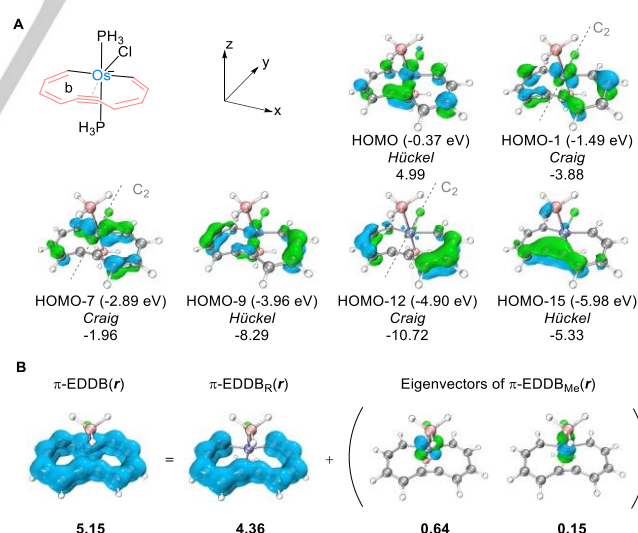


**Figure 4.** (A) The six key occupied  $\pi$ -molecular orbitals of **1a'** displayed (isovalue of 0.06) with the eigenvalues in parentheses on the first line. The types of orbitals (Craig or Hückel) are given on the middle line with the involved  $d_{xz}$  or  $d_{yz}$ , respectively. The NICS(1) $_{\pi,zz}$  values of point b are given on the bottom line. (B) Results of the analysis of  $d$ -orbital contributions to  $\pi$ -EDDB( $r$ ) with the electron populations to **1a'**.

## RESEARCH ARTICLE

The mechanism for the formation of **1** was explored by density functional theory (DFT) calculations. As shown in Figure 5, initially **L**<sub>1</sub> coordinates with osmium to form **A**<sub>1</sub>, and is accompanied by the dissociation of a PPh<sub>3</sub>. Then the PPh<sub>3</sub> nucleophilically attacks the internal carbon of the coordinated alkyne of **A**<sub>1</sub> to form **B**<sub>1</sub>, but no transition state was found for this transaction. The other alkyne subsequently coordinates with the osmium after the chloride atom leaves from the osmium center, affording **C**<sub>1</sub>. A second nucleophilic addition of PPh<sub>3</sub> to the coordinated alkyne then occurs, generating **D**<sub>1</sub>, and again, no transition state was found. Subsequently, the acid facilitated OH<sup>-</sup> departure takes place, forming **E**<sub>1</sub> through the transition state (**TS**<sub>D1-E1</sub>) with an energy barrier of 19.3 kcal/mol. Finally, an acetate-mediated aromatization takes place, leading to the target aromatic osma-dehydro[11]annulene. Overall, the reaction contains an interesting [10+1] cycloaddition process on the basis

of twice nucleophilic attacks of PPh<sub>3</sub> to coordinated alkynes forming two Os–C bonds, and a simultaneous dehydration process catalyzed by acetic acid which is driven by the aromaticity of **1**.

From the proposed mechanism, we realized that the intermediate **D**<sub>1</sub> might be isolated. Initially, we carried out the reaction of **L**<sub>1</sub> with OsCl<sub>2</sub>(PPh<sub>3</sub>)<sub>3</sub>/PPh<sub>3</sub> in the absence of AcOH, however, the expected product **D**<sub>1</sub> could only be detected by ESI-MS but not be purified due to its instability (Figure S72). Further addition of P(OMe)<sub>3</sub> was necessary to give an air stable complex **D**<sub>1</sub>-P(OMe)<sub>3</sub> (88%). This complex could be further converted into **1a** in the yield of 86% upon the addition of HCl (Scheme 2). The only difference of **D**<sub>1</sub>-P(OMe)<sub>3</sub> from **D**<sub>1</sub> is the auxiliary phosphine ligands, therefore, its isolation provides strong evidence for the mechanism shown in Figure 5.

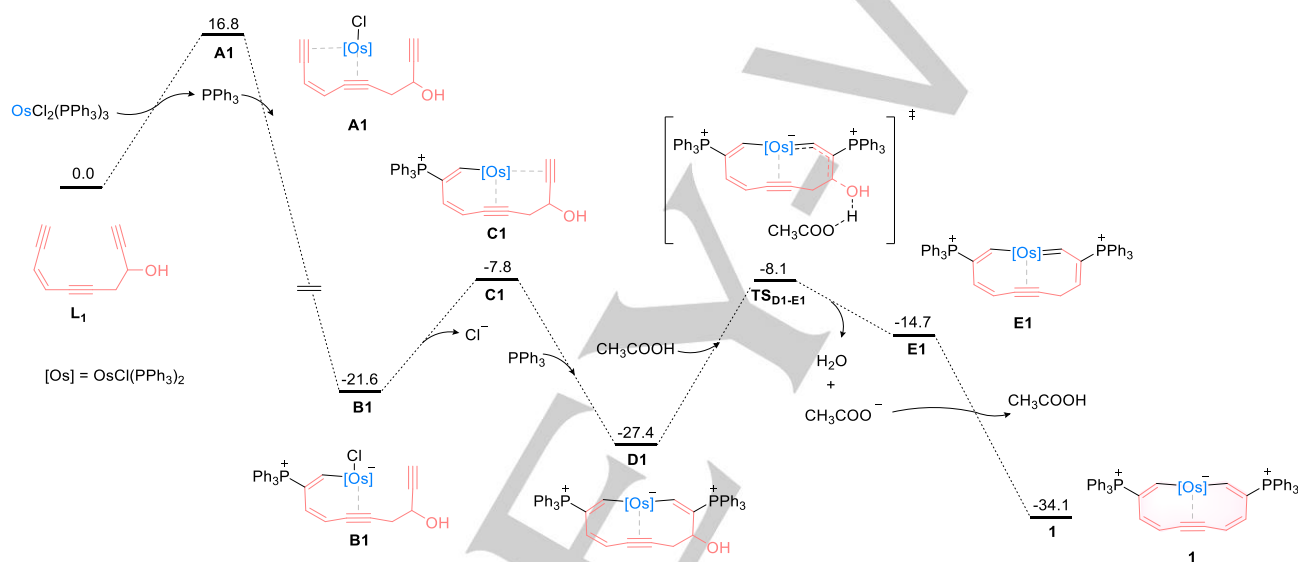


**Figure 5.** Gibbs free energy profile for the DFT-calculated mechanism of the formal [10+1] cycloaddition at 298 K. The computed free energies are in kcal/mol.



**Scheme 2.** The isolation and reactivity of the key intermediate **D**<sub>1</sub>-P(OMe)<sub>3</sub>.

After our successful synthesis and characterization of a series of osma-dehydro[11]annulenes (**1a-1c**) from **L**<sub>1</sub>, we attempted to further increase the diversity of these interesting complexes. When **L**<sub>1</sub> was replaced by **L**<sub>2</sub>, two analogous products (**2a** and **2b**) were produced in the yields of 90% and 94%, respectively (Figure 6).

Similarly, stepwise addition of OsCl<sub>2</sub>(PPh<sub>3</sub>)<sub>3</sub>/PPh<sub>3</sub> and P(OMe)<sub>3</sub> to the fully-conjugated ligand precursor (**L**<sub>3</sub>) produced a

complex (**3a**). In this case, CH<sub>3</sub>COOH was not necessary because there was no dehydration step. When P(OMe)<sub>3</sub> was changed to 2-isocyanonaphthalene, complex **3b** was generated in the same way (Figure 6).

The single-crystal X-ray structures of complexes **2a** and **3a** are shown in Figure 6. Similar to **1a**, each of these species contains a planar 11-membered metalla-cycle. The sum of the internal bond angles in **2a** and **3a** are 1620.0° and 1619.8°,

## RESEARCH ARTICLE

respectively, and the mean deviations of the least-squares planes are 0.000 and 0.028 Å for the 11MRs, respectively, data which are all comparable to those of **1a** and indicate the good planarity. The two  $\alpha$ -protons in the  $^1\text{H}$  NMR spectrum of **2a** appear at 12.99

and 12.88 ppm, and the other two protons on the 11MR are located at 7.39 and 7.19 ppm. Likewise, the two  $\alpha$ -protons in the  $^1\text{H}$  NMR spectrum of **3a** are at 12.84 ppm. All these parameters are very close to those of **1a** and indicate the aromaticity.

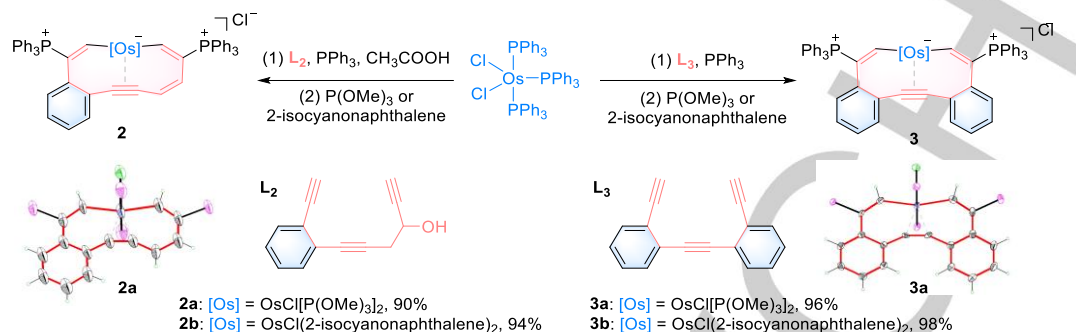


**Figure 6.** Synthesis of osma-dehydrobenzo[11]-annulenes **2** and osma-dehydridibenzo[11]-annulenes **3** and single-crystal X-ray structures for the cations of complexes **2a** and **3a** with thermal ellipsoids drawn at the 50% probability level. Phenyl groups in PPh<sub>3</sub> and methoxy groups in P(OMe)<sub>3</sub> have been omitted for clarity.

The reactivities of these osmadehydro[11]annulenes were next investigated. Due to the similarity, only complex **1c** was chosen as the reactant, for its facile crystallization and characterization compared to other complexes. As discussed above, the aromaticity of these complexes has been confirmed by their structural parameters and spectral data, together with theoretical calculations, therefore, the first tested reactivity was an electrophilic aromatic substitution reaction, which would be helpful for verifying their aromaticity experimentally.<sup>[29]</sup> As shown in Scheme 3a, the respective reactions of **1c** with Br<sub>2</sub> and 1-bromo-3,3-dimethyl-1,3-dihydro-1 $\lambda^3$ -benzo[d][1,2]iodaoxole were carried out in dichloromethane at rt for 12 h. If one equivalent of the bromination reagent was employed, a mixture of monobromo- and dibromo-substituted products would be generated. On the other hand, use of two equivalents of the reagent afforded the dull red dibromo-substituted product **4** cleanly in the yields of 83% and 92%, respectively, and no bromine-addition product was detected (Figure 7). These two reactions are further evidence for the aromaticity of osma-dehydro[11]annulenes.

To explore why these reactions took place at C3 and C8 positions, the condensed dual descriptor (CDD),<sup>[30]</sup> a universal method for predicting the reactivity sites (atoms with the most negative  $\Delta f_k$  value) of electrophilic substitution, was performed on **1c**. The results showed that C3 and C8 of **1c** have the two most negative  $\Delta f_k$  values (-0.100 and -0.093, respectively)

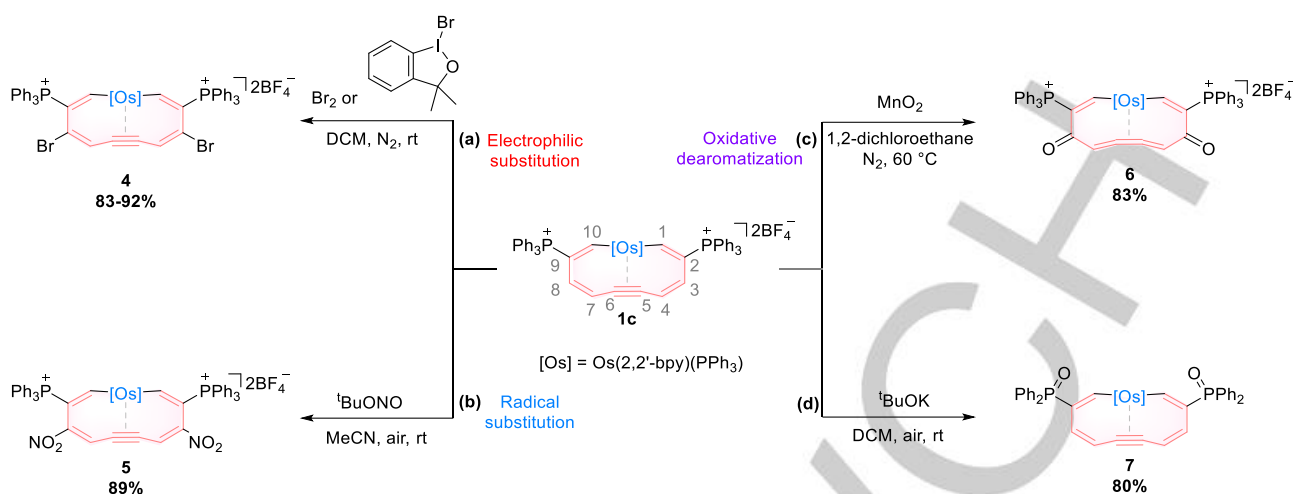
compared to the others (-0.052 ~ +0.095), indicating the strongest nucleophilicity which is favorable for electrophilic reagents.

Complex **1c** is also reactive with <sup>1</sup>BuONO, a popular precursor for radical nitration (Scheme 3b).<sup>[31]</sup> Treatment of **1c** with excess <sup>1</sup>BuONO in acetonitrile at rt under air for 24 h gave the dinitration product **5**. The single-crystal X-ray structure (Figure 7) shows that the nityls are attached at C3 and C8, the same as the bromo-substituted positions.

Complex **1c** was further treated with excess MnO<sub>2</sub> in 1,2-dichloroethane at 60 °C for 2 days, leading to the formation of the red compound **6** (Scheme 3c). The solid structure of **6** (Figure 7) shows it is an eleven-membered osmacycle containing a cumulative triene fragment and two carbonyl groups within the ring. Therefore, **6** is the oxidation product, and its relationship with **1c** is similar to that of benzoquinone with benzene.

When <sup>1</sup>BuOK was added into a solution of **1c** in dichloromethane under air, after 1 day, complex **7** was isolated (Scheme 3d). The structure of **7** (Figure 7) indicates that during the reaction, the PPh<sub>3</sub><sup>+</sup> groups were converted to O=PPh<sub>2</sub> groups (a proposed mechanism is shown in Figure S17).<sup>[32]</sup> In addition, **1c** was stable in the presence of HCl in boiling 1,2-dichloroethane after more than 7 days. Therefore, it can be concluded that the aromatic eleven-membered skeleton exhibit high stability under either basic or acidic conditions.

## RESEARCH ARTICLE



**Scheme 3.** Reactivities of **1c** toward Br<sub>2</sub>, 1-bromo-3,3-dimethyl-1,3-dihydro-1λ<sup>3</sup>-benzo[d][1,2]iodaoxole, Cu(NO<sub>3</sub>)<sub>2</sub>, MnO<sub>2</sub> and <sup>t</sup>BuOK.

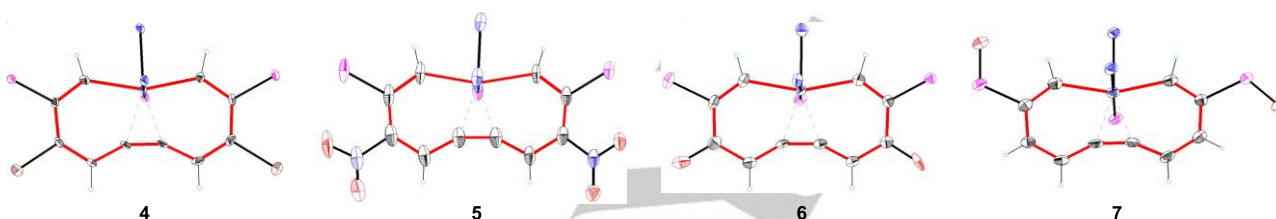


**Figure 7.** Single-crystal X-ray structures for the cations of complexes **4-7** with thermal ellipsoids drawn at the 50% probability level. Phenyl groups in PPh<sub>3</sub> or P(O)Ph<sub>2</sub> and C, H atoms in 2,2'-dipyridine have been omitted for clarity.

The UV/vis-NIR absorption spectra of all complexes were examined (Figure S18). The representative spectra of **1a**, **1c**, **2a**, **3a** and **5**, together with their structures, are shown in Figures 8A and B, and their absorption maxima in low-energy band are at 463, 495, 494, 488 and 743 nm with molar absorption coefficient values ( $\epsilon$ ) of 11810, 12433, 7360, 9796 and 13832 M<sup>-1</sup>·cm<sup>-1</sup>, respectively. Interestingly, the absorption of nitro-substituted complex **5** is significantly different from those of other complexes. Not only does its maximum absorption peak is red-shifted by more than 200 nm, but it also exhibits full-band absorption in the visible light region, with a molar absorption coefficient of 4177 M<sup>-1</sup>·cm<sup>-1</sup> at 600 nm at the lowest point.

To gain more insight into the largely different UV/vis-NIR absorption between **1c** and **5**. The time-dependent density functional theory (TD-DFT) calculations were carried out.<sup>[33]</sup> Figure 8C presents the first ten excited states of **1c** (red circle) and **5** (purple triangle) with corresponding oscillator strength ( $f$ ). As shown in Figure 8D, the calculated absorption peaks of the first excited states locate at 724 and 742 nm for complexes **1c**

and **5**, respectively, both relating to the transitions of HOMO–LUMO. However, their  $f$  values are far different (0.0027 for **1c** and 0.2578 for **5**), which explains why there is almost no absorption around 700 nm for **1c**. Notably, for **1c**, the HOMO and LUMO are mainly distributed on two different frameworks, the 11-membered ring and 2,2'-bipyridine, respectively, leading to a charge transfer transition (CT), while for complex **5** with two strong electron-withdrawing nitril groups, both of HOMO and LUMO are mainly distributed on the 11-membered ring, resulting in a local excitation (LE) (Figures 8E and S16). Additionally, the calculated main absorption peaks for **1c** locate at 487 and 475 nm, corresponding to the second and third excited states, with  $f$  values of 0.1439 and 0.0495, respectively. These two excited states both correlate with the transitions from HOMO to LUMO+1 and HOMO to LUMO+2. In comparison, the other calculated main absorption peak for **5** is at 489 nm ( $f = 0.2718$ ), which corresponds to the fourth excited states, relating to the transitions of HOMO–LUMO and HOMO–2–LUMO. The theoretical results are consistent with the experimental results.

## RESEARCH ARTICLE

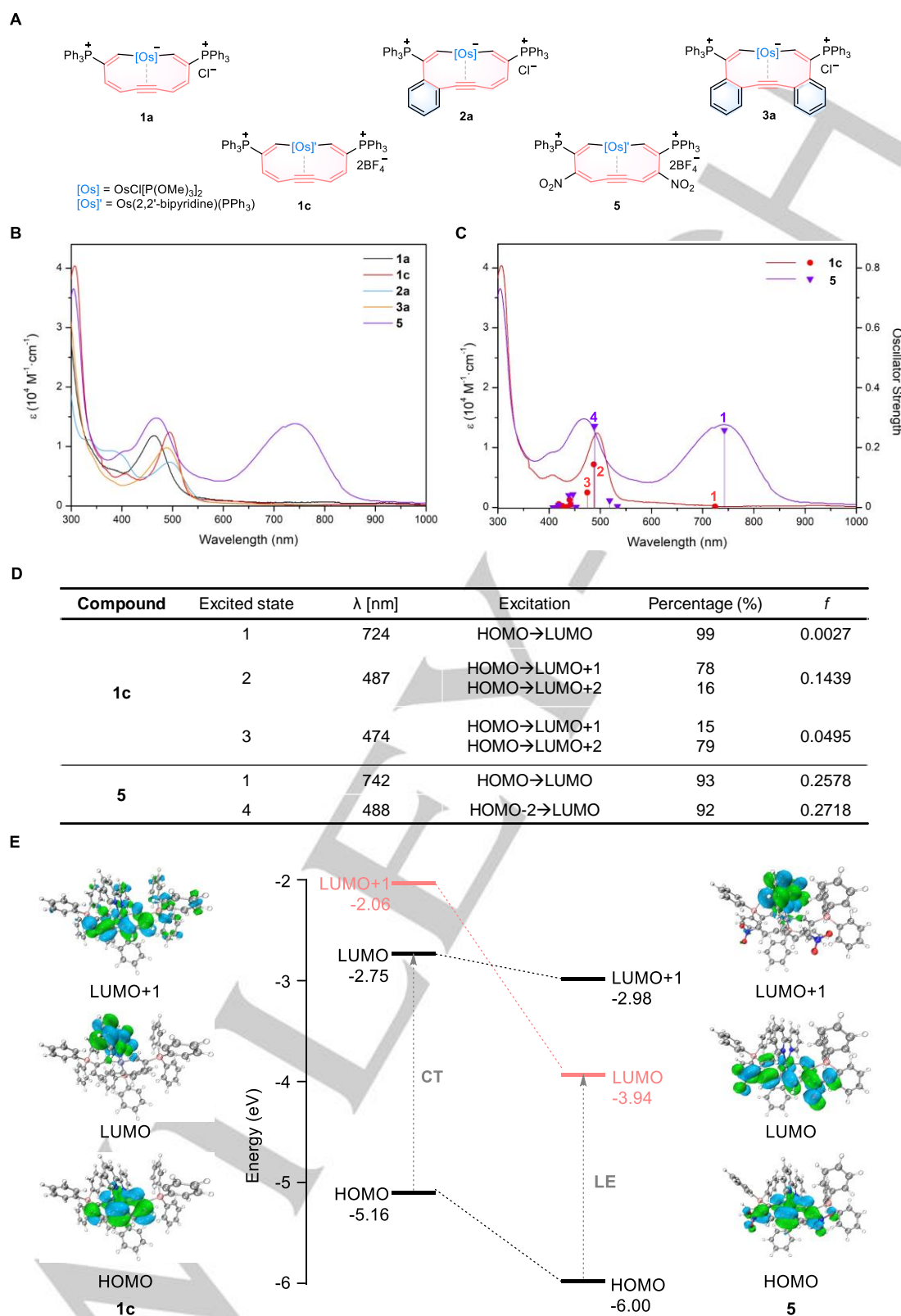


**Figure 8.** (A) Structures of **1a**, **1c**, **2a**, **3a** and **5**. (B) UV/Vis-NIR absorption spectra of **1a**, **1c**, **2a**, **3a** and **5**, measured in acetonitrile at rt. (C) The first ten excited states of **1c** (red circle) and **5** (purple triangle) calculated by TD-DFT and the UV/Vis-NIR absorption spectra of **1c** and **5** measured in acetonitrile at rt. (D) DFT calculated excited wavelength ( $\lambda$ ) and oscillator strengths ( $f$ ) of **1c** and **5**. (E) The HOMO, LUMO and LUMO+1 of **1c** (left) and **5** (right) with the corresponding eigenvalues given in the middle diagram.

## RESEARCH ARTICLE

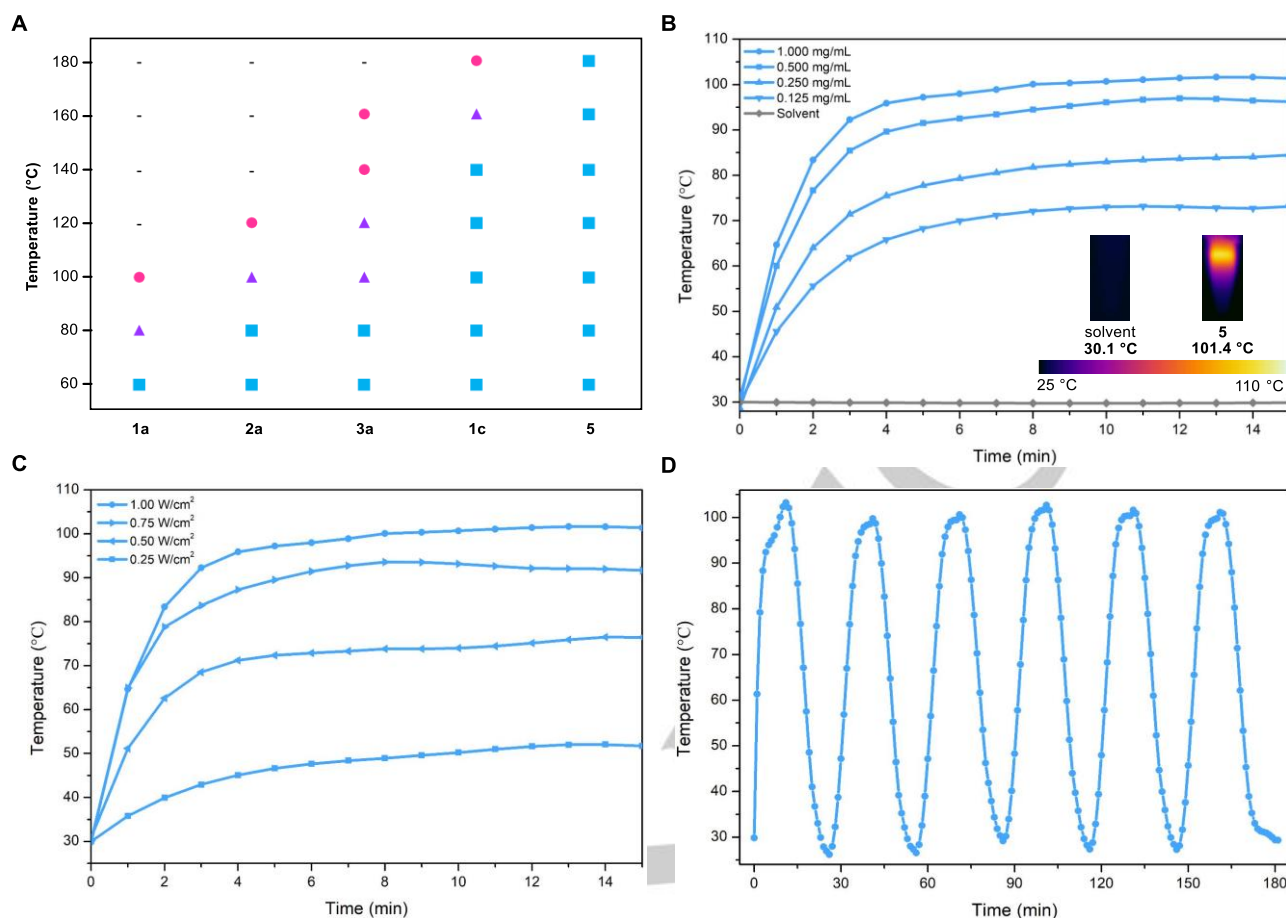


**Figure 9.** (A) Thermal stabilities of **1a**, **2a**, **3a**, **1c** and **5** in the solid state, and all tests were carried out for 3 hours in air, ■ = stable, ▲ = partly decomposed, ● = completely decomposed. (B) Photothermal conversion of **5** at different concentrations (0.125–1.000 mg mL<sup>-1</sup>) and of solvent under 808 nm (1 W cm<sup>-2</sup>) laser irradiation for 15 min and infrared imaging of solvent and **5** (1.000 mg mL<sup>-1</sup>). (C) Photothermal conversion of **5** (1.000 mg mL<sup>-1</sup>) under 808 nm laser irradiation with different exposure intensity (0.25–1.00 W cm<sup>-2</sup>). (D) Photothermal stability of **5** (0.500 mg mL<sup>-1</sup>) alone upon 808 nm (1.00 W cm<sup>-2</sup>) laser irradiation for six on/off cycles.

The stabilities of complexes **1a**, **2a**, **3a**, **1c** and **5** under air atmosphere were finally assessed (Figure 9A). In the solid state, all these compounds are stable at rt. When the temperature was increased to 80 °C, complex **1a** started to decompose, and it was completely decomposed at 100 °C. Complexes **2a** and **3a** are more stable, and their decomposition temperatures are ~100 °C (complete decomposition temperatures are 120 and 140 °C, respectively). The results suggest that as the number of fused rings in the compounds increases, the structures become more stable, consistent with the normal stability sequence for organic dehydroannulenes.<sup>[19]</sup> Complexes **1c** and **5**, each of which contains a bidentate 2,2'-bipyridine ligand, are the most stable species. They could be stored at rt for at least 2 months, and did not decompose at 140 °C. Specifically, no decomposition was detected for **5** even at 180 °C.

Due to the superior thermal stability and broad UV/vis-NIR absorption of complex **5**, it might be used as a photothermal medium. Therefore, we studied the photothermal properties of **5** under 808 nm laser irradiation. As shown in Figure 9B, the DMF solutions of complex **5** with different concentrations all showed significant temperature rise under laser irradiation. When the

concentration was 1.000 mg/mL, and the exposure intensity of the laser was 1.00 W/cm<sup>2</sup>, the temperature rose from 30 °C to 82.6 °C within two minutes, and finally reached to 101.4 °C. In comparison, the temperature of pure solvent remained around 30 °C under the same conditions. Clear difference could be seen from the corresponding infrared images shown in the same figure. The correlation between the maximum temperature, the concentration (Figure 9B), and the laser energy density (Figure 9C) indicates its adjustable photothermal performance. Further photothermal stability experiments were conducted as shown in Figure 9D. No significant degradation was observed during six heating and cooling cycles, confirming its potential as a photothermal material.

The electrochemical properties of these osma-dehydro[11]annulenes were further examined. As shown in Figure 10, there is one reversible oxidation-reduction couples for each of complexes **1a**, **2a**, **3a** and **1c**, with the half-wave potentials ( $E_{1/2}$ ) of 0.33, 0.32, 0.41 and 0.80 V, respectively. In contrast, complex **5** has three reversible oxidation-reduction couples, and the  $E_{1/2}$  are at 1.29, -0.18 and -0.36 V. In general, the oxidation and reduction potentials of the metalla-dehydro[11]annulenes can be adjusted in a wide range by changing the size and the substituent

## RESEARCH ARTICLE

group on the conjugated system, or the ligands on the metal (for more details, see Figure S19).

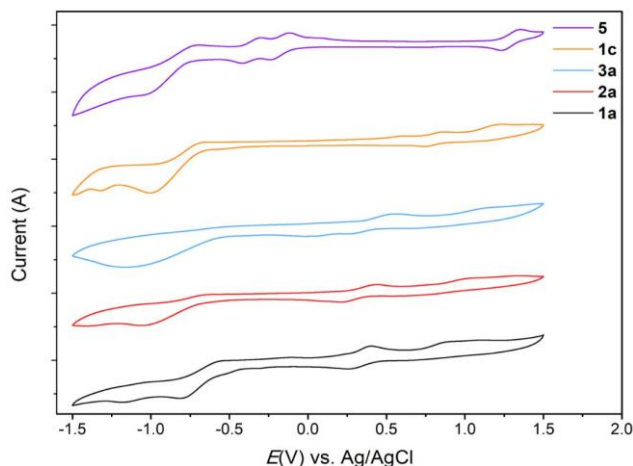


**Figure 10.** Cyclic voltammograms of **1a**, **2a**, **3a**, **1c** and **5** in  $\text{CH}_2\text{Cl}_2$ .

## Conclusion

We have synthesized a series of osma-dehydro[11]annulenes, which are the first mononuclear aromatic metalla-[ $n$ ]annulene derivatives with a ring size larger than 6, by the reactions of 10-carbon-chain ligand precursors with a commercially available osmium reagent. The reactions were one-pot in nature, and the products were isolated in high yields. These complexes show good air, water and thermal stability. With Craig-Hückel hybrid aromaticity, but dominated by Craig aromaticity, their aromatic nature was revealed by CMO-NICS and EDDB computations. Photophysical and electrochemical studies indicate they have potential application values in material science, for their easily adjustable UV/vis-NIR absorption and electrochemical properties, and adjustable photothermal behavior. This work provides an opportunity for the construction of large aromatic metalla-annulenes with different ring sizes, which could be significant in the further development of metalla-aromatic chemistry.

## Acknowledgements

This work was supported by the National Natural Science Foundation of China (Nos. 21931002, 22371111, 22071098 and 22101123), the Guangdong Provincial Key Laboratory of Catalysis (No. 2020B121201002), Introduction of Major Talent Projects in Guangdong Province (No. 2019CX01C079), Guangdong Grants (No. 2021ZT09C064), and Outstanding Talents Training Fund in Shenzhen.

## Conflict of Interest

The authors declare no conflict of interest.

## Data Availability Statement

The data that support the findings of this study are available in the supplementary material of this article. Deposition Numbers 2226300 (for **1a**), 2226301 (for **1b**), 2226296 (for **1c**), 2226294 (for **2a**), 2226297 (for **2b**), 2226298 (for **3a**), 2226295 (for **3b**), 2226299 (for **4**), 2305708 (for **5**), 2305709 (for **6**), 2305707 (for **7**) contain the supplementary crystallographic data for this paper. These data are provided free of charge by the joint Cambridge Crystallographic Data Centre and Fachinformationszentrum Karlsruhe Access Structures service.

**Keywords:** Metallacycles • Annulene • Aromaticity •  $d_{\pi}\text{-}p_{\pi}$  Conjugation • [10+1] Cycloaddition reaction

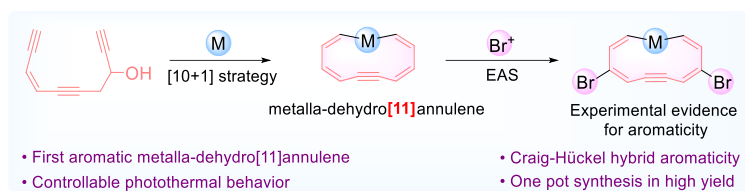
- C. Liu, Y. Ni, X. Lu, G. Li, J. Wu, *Acc. Chem. Res.* **2019**, *52*, 2309-2321.
  - K. Parmar, C. S. Blaquiere, B. E. Lukan, S. N. Gengler, M. Gravel, *Nat. Synth.* **2022**, *1*, 696-700.
  - Z. Miao, S. A. Gonsales, C. Ehm, F. Mentink-Vigier, C. R. Bowers, B. S. Sumerlin, A. S. Veige, *Nat. Chem.* **2021**, *13*, 792-799.
  - S. Moles Quintero, M. M. Haley, M. Kertesz, J. Casado, *Angew. Chem. Int. Ed.* **2022**, *61*, e202209138; *Angew. Chem.* **2022**, *134*, e202209138.
  - M. Iyoda, J. Yamakawa, M. J. Rahman, *Angew. Chem. Int. Ed.* **2011**, *50*, 10522-10533; *Angew. Chem.* **2011**, *123*, 10708-10740.
  - Z. S. Yoon, A. Osuka, D. Kim, *Nat. Chem.* **2009**, *1*, 113-122.
  - C. D. Stevenson, *Acc. Chem. Res.* **2007**, *40*, 703-711.
  - E. L. Spitzer, C. A. Johnson II, M. M. Haley, *Chem. Rev.* **2006**, *106*, 5344-5386.
  - I. Hisaki, M. Sonoda, Y. Tobe, *Eur. J. Org. Chem.* **2006**, 833-847.
  - M. J. Marsella, *Acc. Chem. Res.* **2002**, *35*, 944-951.
- C. Gellini, P. R. Salvi, *Symmetry* **2010**, *2*, 1846-1924.
  - I. Casademont-Reig, E. Ramos-Cordoba, M. Torrent-Sucarrat, E. Matito, *Molecules* **2020**, *25*, 711.
  - I. Casademont-Reig, E. Ramos-Cordoba, M. Torrent-Sucarrat, E. Matito, *Aromaticity: Modern Computational Methods and Applications Aromaticity descriptors based on electron delocalization*, Elsevier, Amsterdam, **2021**, pp. 235-258.
- E. Hückel, *Z. Phys.* **1931**, *70*, 204-286.
- E. Heilbronner, *Tetrahedron Lett.* **1964**, *5*, 1923-1928.
- J. M. Mercero, A. I. Boldyrev, G. Merino, J. M. Ugalde, *Chem. Soc. Rev.* **2015**, *44*, 6519-6534.
  - D. Y. Zubarev, B. B. Averkiev, H. J. Zhai, L. S. Wang, A. I. Boldyrev, *Phys. Chem. Chem. Phys.* **2008**, *10*, 257-267.
  - T. M. Krygowski, H. Szatyłowicz, O. A. Stasyuk, J. Dominikowska, M. Palusiak, *Chem. Rev.* **2014**, *114*, 6383-6422.
  - M. D. Watson, A. Fechtenkötter, K. Müllen, *Chem. Rev.* **2001**, *101*, 1267-1300.
  - M. Solà, *Nat. Chem.* **2022**, *14*, 585-590.
  - Z. Zeng, X. Shi, C. Chi, J. T. López Navarrete, J. Casado, J. Wu, *Chem. Soc. Rev.* **2015**, *44*, 6578-6596
- D. Ajami, O. Oeckler, A. Simon, R. Herges, *Nature* **2003**, *426*, 819-821.
- D. P. Craig, N. L. Paddock, *Nature* **1958**, *181*, 1052-1053.
- L. Chen, L. Lin, A. R. Nath, Q. Zhu, Z. Chen, J. Wu, H. Wang, Q. Li, W.-F. Lin, J. Zhu, J. Xia, *Proc. Natl. Acad. Sci. U. S. A.* **2023**, *120*, e2215900120.
- D. L. Thorn, R. Hoffmann, *Nouv. J. Chim.* **1979**, *3*, 39-45.
- D. Chen, Y. Hua, H. Xia, *Chem. Rev.* **2020**, *120*, 12994-13086.
  - b) B. J. Frogley, L. J. Wright, *Chem. Eur. J.* **2018**, *24*, 2025-2038.
  - c) I. Fernández, G. Frenking, G. Merino, *Chem. Soc. Rev.* **2015**, *44*, 6452-6463.
  - d) J. Chen, G. Jia, *Coord. Chem. Rev.* **2013**, *257*, 2491-2521.
  - e) W. Ma, C. Yu, T. Chen, L. Xu, W. X. Zhang, Z. Xi, *Chem. Soc. Rev.* **2017**, *46*, 1160-1192.
  - f) M. Cui, R. Lin, G. Jia, *Chem. Asian J.* **2018**, *13*, 895-912.
  - g) Z. J. Lv, Z. Huang, J. Shen, W. X. Zhang, Z. Xi, *J. Am. Chem.*

## RESEARCH ARTICLE

- Soc. **2019**, *141*, 20547-20555. h) J. Wei, W. X. Zhang, Z. Xi, *Chem. Sci.* **2018**, *9*, 560-568.
- [11]. J. Wei, Y. Zhang, Y. Chi, L. Liu, W. X. Zhang, Z. Xi, *J. Am. Chem. Soc.* **2016**, *138*, 60-63.
- [12]. a) J. Chen, K. H. Lee, H. H. Y. Sung, I. D. Williams, Z. Lin, G. Jia, *Angew. Chem. Int. Ed.* **2016**, *55*, 7194-7198; *Angew. Chem.* **2016**, *128*, 7310-7314. b) S. Zheng, Z. Chu, K. H. Lee, Q. Lin, Y. Li, G. He, J. Chen, G. Jia, *ChemPlusChem* **2019**, *84*, 85-91.
- [13]. C. Castro, W. L. Karney, *J. Phys. Org. Chem.* **2012**, *25*, 612-619.
- [14]. J. C. Babón, M. A. Esteruelas, A. M. López, E. Oñate, *Organometallics* **2022**, *41*, 2513-2524.
- [15]. A. Krebs, J. Wilke, *Top. Curr. Chem.* **1983**, *109*, 189-233.
- [16]. M. Lamač, A. Spannenberg, H. Jiao, S. Hansen, W. Baumann, P. Arndt, U. Rosenthal, *Angew. Chem. Int. Ed.* **2010**, *49*, 2937-2940; *Angew. Chem.* **2010**, *122*, 2999-3002.
- [17]. C. Lefeber, A. Ohff, A. Tillack, W. Baumann, R. Kempe, V. V. Burlakov, U. Rosenthal, *J. Organomet. Chem.* **1995**, *501*, 189-194.
- [18]. a) G. P. Elliott, W. R. Roper, J. M. Waters, *J. Chem. Soc. Chem. Commun.* **1982**, 811-813. b) G. P. Elliott, N. M. McAuley, W. R. Roper, *Inorg. Synth.* **1989**, *26*, 184-189.
- [19]. C. E. F. Rickard, W. R. Roper, S. D. Woodgate, L. J. Wright, *Angew. Chem. Int. Ed.* **2000**, *39*, 750-752; *Angew. Chem.* **2000**, *112*, 766-768.
- [20]. G. R. Clark, L. A. Ferguson, A. E. McIntosh, T. Söhnel, L. J. Wright, *J. Am. Chem. Soc.* **2010**, *132*, 13443-13452.
- [21]. L. J. Wright, *Dalton Trans.* **2006**, 1821-1827.
- [22]. H. Fallah-Bagher-Shaidaei, C. S. Wannere, C. Corminboeuf, R. Puchta, P. v. R. Schleyer, *Org. Lett.* **2006**, *8*, 863-866.
- [23]. a) J. N. A. F. Gomez, R. B. Mallion, *Chem. Rev.* **2001**, *101*, 1349-1384. b) P. Lazzeretti, *Phys. Chem. Chem. Phys.* **2004**, *6*, 217-223. c) J. Poater, M. Solà, R. G. Viglione, R. Zanasi, *J. Org. Chem.* **2004**, *69*, 7537-7542. d) C. Foroutan-Nejad, S. Shahbazian, F. Feixas, P. Rashidi-Ranjbar, M. Solà, *J. Comput. Chem.* **2011**, *32*, 2422-2431. e) S. S. Batsanov, *Inorg. Mater.* **2001**, *37*, 871-885.
- [24]. D. Geuenich, K. Hess, F. Köhler, R. Herges, *Chem. Rev.* **2005**, *105*, 3758-3772.
- [25]. a) S. Klod, E. Kleinpeter, *J. Chem. Soc., Perkin Trans.* **2001**, *2*, 1893-1898. b) Z. Liu, T. Lu, Q. Chen, *Carbon* **2020**, *165*, 468-475.
- [26]. P. v. R. Schleyer, F. Pühlhofer, *Org. Lett.* **2002**, *4*, 2873-2876.
- [27]. Z. Chen, C. S. Wannere, C. Corminboeuf, R. Puchta, P. v. R. Schleyer, *Chem. Rev.* **2005**, *105*, 3842-3888.
- [28]. a) D. W. Szczepanik, M. Andrzejak, K. Dyduch, E. Zak, M. Makowski, G. Mazur, J. Mrozek, *Phys. Chem. Chem. Phys.* **2014**, *16*, 20514-20523. b) D. W. Szczepanik, M. Andrzejak, J. Dominikowska, B. Pawelek, T. M. Krygowski, H. Szatyłowicz, M. Solà, *Phys. Chem. Chem. Phys.* **2017**, *19*, 28970-28981.
- [29]. a) T. B. Wen, S. M. Ng, W. Y. Hung, Z. Y. Zhou, M. F. Lo, L. Y. Shek, I. D. Williams, Z. Lin, G. Jia, *J. Am. Chem. Soc.* **2003**, *125*, 884-885. b) W. Y. Hung, B. Liu, W. Shou, T. B. Wen, C. Shi, H. H. Y. Sung, I. D. Williams, Z. Lin, G. Jia, *J. Am. Chem. Soc.* **2011**, *133*, 18350-18360. c) Y. Cai, Y. Hua, Z. Lu, Q. Lan, Z. Lin, J. Fei, Z. Chen, H. Zhang, H. Xia, *Proc. Natl. Acad. Sci. U. S. A.* **2021**, *118*, e2102310118.
- [30]. a) C. Morell, A. Grand, A. Toro-Labbé, *J. Phys. Chem. A* **2005**, *109*, 205-212. b) C. Morell, A. Grand, A. Toro-Labbé, *Chem. Phys. Lett.* **2006**, *425*, 342-346. c) B. Wang, C. Rong, P. K. Chattaraj, S. Liu, *Theor. Chem. Acc.* **2019**, *138*, 124. d) F. Zielinski, V. Tognetti, L. Joubert, *Chem. Phys. Lett.* **2012**, *527*, 67-72.
- [31]. S. Z. Song, Y. R. Dong, G.P. G. Q. Li, W. T. Wei, *Synthesis* **2020**, *52*, 796-806.
- [32]. S. Xu, H. Huang, Z. Yan, Q. Xiao, *Org. Lett.* **2019**, *21*, 10018-10022.
- [33]. C. Adamo, D. Jacquemin, *Chem. Soc. Rev.* **2013**, *42*, 845-856.

## RESEARCH ARTICLE

## Entry for the Table of Contents



A series of metalla-dehydro[11]annulenes with Craig-Hückel hybrid aromaticity, were constructed by a one pot [10+1] strategy. They are the first monometallic aromatic metalla-[n]annulenes with the ring size larger than 6, and their special aromaticity was confirmed both experimentally and theoretically. This work provides a method to construct large metalla-annulenes with different ring sizes, which is significant for metalla-aromatic chemistry.